

# SYNCHRONOUS THERMAL INSTABILITY PREDICTION FOR OVERHUNG ROTORS

by

**R. Gordon Kirk**

Professor, Mechanical Engineering Department

Director, Rotor Dynamics Laboratory

**Zenglin Guo**

Post-Doctorate Research Engineer, Rotor Dynamics Laboratory

and

**Avinash C. Balbahadur**

Graduate Research Assistant, Rotor Dynamics Laboratory

Virginia Tech

Blacksburg, Virginia



*R. Gordon Kirk is Professor of Mechanical Engineering and Director of the Rotor Dynamics Laboratory at Virginia Polytechnic Institute and State University, also known as Virginia Tech, in Blacksburg, Virginia. He previously had 13 years' industrial experience in both aircraft and heavy land-based rotating machinery with Pratt & Whitney Aircraft and Ingersoll-Rand Turbo Products. Dr. Kirk established the Rotor Dynamics Laboratory Industry Affiliates Group shortly*

*after coming to Virginia Tech in 1985. He has published over 100 technical papers in the area of rotating machinery dynamic analysis and teaches the Introduction to Rotor Dynamics graduate level course at Virginia Tech. Dr. Kirk has organized the Rotating Structure and Machinery sessions for the ASME Design Technical Vibrations Conference for 1995, 1997, 1999, and 2001.*

*Dr. Kirk received his BSME (1967), MSME (1969), and Ph.D. (1972) degrees from the University of Virginia. He is a registered Professional Engineer in the State of Virginia.*



*Zenglin Guo is a Post-Doctorate Research Engineer at Virginia Tech Rotor Dynamics Laboratory, in Blacksburg, Virginia. He was an Associate Professor of Xi'an Jiaotong University before he came to Virginia Tech in 2000. Dr. Guo has published more than 20 technical papers in the area of rotorbearing dynamics.*

*Dr. Guo received his B.S. (1984) and M.S. (1987) degrees from Tianjin University. In 1997, he received his Ph. D.*

*degree in Mechanology from Xi'an Jiaotong University.*



*Avinash C. Balbahadur was a Graduate Research Assistant with Virginia Tech Rotor Dynamics Laboratory, in Blacksburg, Virginia, at the time this paper was written. He graduated from Dartmouth College with an A.B. degree (Engineering Sciences, 1995) and a B.E. degree (Chemical Engineering). He subsequently completed an M.S. degree (Mechanical Engineering, 1997) at the same institution.*

*Dr. Balbahadur received his Ph. D. degree (2001) from Virginia Tech.*

*Dr. Balbahadur is now with Siemens Westinghouse Power Corporation, in Orlando, Florida.*

## ABSTRACT

Rotor thermal bending is a complicated phenomenon that can lead to unstable spiral vibrations. This phenomenon is primarily due to a temperature difference developing across the journal. The temperature difference can either be caused by the journal rubbing against stationary components or by viscous shearing within the lubricant. The latter mechanism is often referred to as the Morton effect. In this paper, a theoretical model has been developed for a synchronous thermal instability that is caused by differential viscous shearing in bearings of overhung rotors. This model employs an unbalance threshold criterion for instability prediction instead of using a traditional frequency-domain stability analysis. The computer program, which is based on the theoretical model, has been further developed to examine various cases that pertain to this thermal instability. The case studies presented in this paper include rotors supported by fixed geometry design bearings and tilting pad journal bearings. The results are discussed and show good agreement between the theoretical predictions and the practical observations.

## INTRODUCTION

Rotor thermal bending is a complicated phenomenon that can lead to unstable spiral vibrations (Schmied, 1987). This phenomenon is primarily due to a temperature difference developing across the journal. The temperature difference can either be caused by the journal rubbing against stationary components or by viscous shearing within the lubricant. The former mechanism was first noticed by Newkirk (1926) and later analyzed by Dimarogonas (1973). This mechanism is called the Newkirk effect. The latter mechanism has recently been studied (Keogh and Morton, 1994) and is often referred to as the Morton effect.

Within the last decade much interest has been shown on the Morton effect induced thermal instability. Recent theoretical (Keogh and Morton, 1994) and experimental (de Jongh and Morton, 1994; Faulkner, et al., 1997a, 1997b) studies have focused on this problem. However, most of the theoretical work has been done using complex analysis, and limited comparison between experimental and theoretical research has been made. This paper presents a theoretical model for overhung rotor thermal instability analysis based upon steady-state mechanical response coupled to an approximate fluid thermal analysis for a whirling journal.

The Morton effect can most easily occur when the journal is executing a synchronous orbit around the bearing center. This centered orbit causes one portion of the journal surface to always be at the minimum film thickness, while a diametrically opposite section of the journal surface is always at the maximum film thickness. Lower film thickness areas are generally associated with higher viscous shear stresses that produce higher temperatures. As a result, a hot spot will develop on the journal surface exposed to the minimum film thickness region, and a cold spot will be formed on the surface at maximum film thickness. This leads to a temperature gradient developing across the journal. Such a gradient may create a thermal imbalance from the thermal bending that occurs across the shaft at the journal location. Under these conditions the bent shaft will decrease the bearing clearance and elevate the thermal gradient. The increased temperature gradient will then initiate more thermal bending. These actions describe a positive feedback mechanism that will drive the system unstable, producing very large synchronous response.

The occurrence of such synchronous vibration excursions may be caused by more than one mechanism. For hot machines, the impeller or disk may be forced to move off-center due to nonuniform slip in the centering mechanism, or the disk may simply become loose and move eccentric. A hard mechanical rub may also cause local heating and bending of the rotor, resulting in a mechanical imbalance. The concept of a thermal heating, caused by a hydrodynamic fluid-film bearing, is the key element that drives the thermal instability known as the Morton effect. It may be very difficult to clearly distinguish between a loose impeller and a fluid shear produced imbalance. The two part paper by Faulkner, et al. (1997a, 1997b), describe a field problem for a gas engine turbocharger that first experienced a mechanical looseness excited vibration and then a Morton effect vibration. Mechanical looseness can be proven by match-marking or other methods of detecting impeller or disk movement, either axially or circumferentially. This may not be an easy procedure in real machinery. To predict thermal instability was also not an easy exercise in the mid 1990s. The results of the 1997 Faulkner, et al. (1997a, 1997b), papers describe the confusion and final resolution of a classic example of both impeller looseness and Morton effect vibration. The reduced data for the Morton effect vibration is shown in Figures 1 and 2 and illustrates how the instability onset may occur. The pulsating synchronous vibration may build over several minutes and be accompanied by phase shifting. The clear indication of a speed onset can be observed by noting the speeds at which the vibration pulsations increase and when they are suppressed.

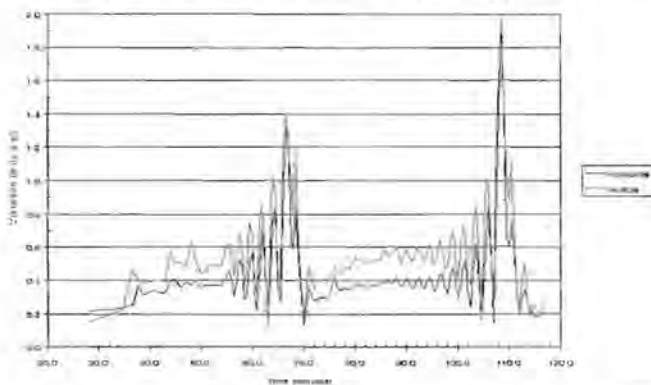


Figure 1. Measured Shaft Amplitude Versus Time for Modified Upgrade Turbine. (Courtesy Faulkner, et al., 1997b)

The instability was eliminated by a bearing modification to make the design have a higher operating eccentricity ratio (Figure 3). The low residual imbalance of the machine was also considered to be essential in the resolution of the vibration problem. Larger vibration levels will lift the bearing journals in a more nearly centered orbit and negate the improvement from the larger static operating eccentricity ratio.

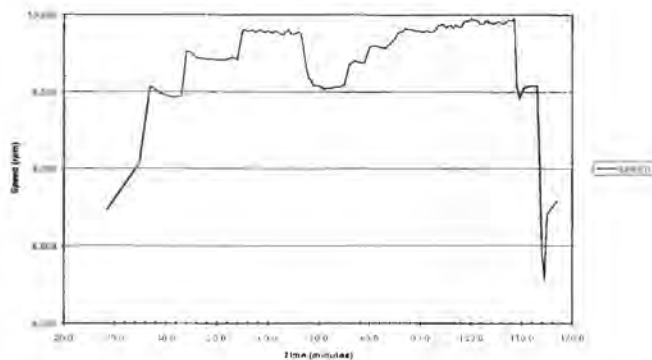


Figure 2. Measured Service Speed Versus Time for Modified Upgrade Turbine. (Courtesy Faulkner, et al., 1997b)

#### Turbine Bearing Shaft Vibration at 1xSS

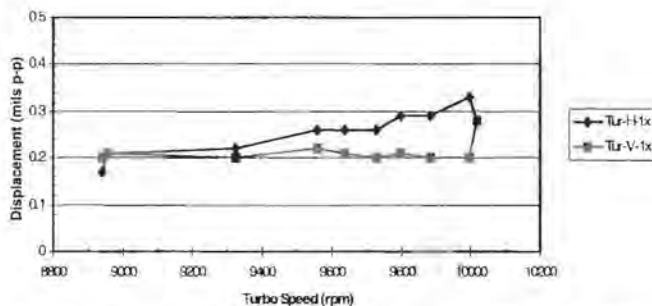


Figure 3. Measured Shaft Amplitude Versus Speed for Modified Upgrade Turbine with Modified Bearing. (Courtesy Faulkner, et al., 1997b)

Most of the prior models of the Morton effect have involved complex stability analyses (Keogh and Morton, 1994; Larsson, 1999a, 1999b). In these models, an initial deformed rotor configuration is assumed and is then used as an input in a dynamic model of the rotor system. This dynamic model produces a synchronous orbit that causes a circumferential temperature distribution to develop on portions of the shaft within the bearings. A thermal bend, which depends on the temperature distribution and the rotor thermal characteristics, is subsequently initiated. This thermal bend affects the rotordynamics and gives rise to the positive feedback behavior. The stability of the resulting feedback transfer function can then be analyzed by using Nyquist plots or another equivalent method.

In real machines satisfactory performance is established by using specified vibration or unbalance threshold levels that are given in standards published by various organizations. One method of specifying such levels is to restrict the maximum allowable centrifugal force that acts on the machine. This restriction then limits the allowable imbalance for each speed value. Such a criterion determines whether the rotor will be "stable" or "unstable" during operation, i.e., if the total mechanical and thermal unbalance level exceeds the threshold level given by the allowable imbalance then the rotor will be "unstable." This notion of practical stability will be utilized in the model presented in this paper.

The current model for the Morton effect first requires an estimate for the initial mechanical imbalance in the rotor. This imbalance is then put into the dynamic rotor model to obtain the synchronous orbit. A fluid film bearing model is then used to establish the temperature distribution that leads to the thermal imbalance. Finally, an unbalance threshold criterion is used to determine the system stability (Balbahadur and Kirk, 2002a, 2002b).

## THEORETICAL MODEL

The solution procedure by the practical stability method consists of the following steps:

1. Determine the film thickness for the specific bearing type.
2. Solve for the static equilibrium position of the journal.
3. Predict the steady-state orbit at the journal for an assumed imbalance.
4. Determine the hot and cold spot regions for the journal.
5. Evaluate the temperature distribution in the journal.
6. Compute the rotor thermal bend for the steady-state condition.
7. Calculate the total imbalance resulting from the average hot spot temperature gradient.
8. Compare the total imbalance to the stability threshold.

The following discussion presents the basic equations necessary to implement the previous outline of the essential steps. First, the film thickness expressions must be known. Cameron (1966) gives the film thickness for a plain journal bearing as:

$$h = C_b [1 + e \cos(\xi)] \quad (1)$$

The following film thickness expression has been derived for the tilting pad journal bearings (Balbahadur and Kirk, 2002a):

$$h = (R_p - R_j) + e \cos(\theta_c - \theta) - (R_p - R_b) \cos(\theta - \theta_p) - \delta (R_p + r_p) \sin(\theta - \theta_p) \quad (2)$$

This expression agrees well with the one provided by Monmousseau, et al. (1997). In Equation (2),  $R_p$  = pad radius of curvature,  $\theta_c$  = angle to line joining journal center to bearing center,  $\delta$  = tilt angle,  $\delta_p$  = pivot angular position, and  $r_p$  = pad thickness.

Next the static equilibrium position must be known. A narrow bearing assumption has been used for the fixed geometry journal bearing case. Such an assumption enabled the use of an analytical solution (Cameron, 1966) for the static eccentricity ratio and the static attitude angle. However, due to the complexity of the tilting pad bearings, it is necessary to numerically compute the static equilibrium position for this type bearing. This computation by finite element method involves the balancing of the vertical and horizontal forces acting on the journal and the equilibrium of the moments acting on the pads. The resulting system of equations is then solved using the Newton-Raphson method.

For the third step of the analysis, the synchronous orbit of the journal must be known for an assumed initial mechanical imbalance. The proposed solution method requires the calculation of the rotor response for a specified initial mechanical imbalance,  $U_m$ . This mechanical imbalance will be defined as the imbalance created from a centrifugal force equal to 10 percent of the total static rotor weight. The journal will traverse an elliptical path around its static equilibrium position,  $O_{j0}$  (refer to Figure 4). Once this orbit is known, a general point,  $P$ , on the surface of the journal will also travel along an elliptical path. With reference to Figure 4, the path taken by the general point  $P(x, y)$  on the journal surface can be mathematically described as:

$$\left. \begin{aligned} x &= e_0 \cos(\theta_{j0}) + A_x \cos(\omega t + \phi_x) + R_j \cos(\omega t + \lambda) \\ y &= e_0 \sin(\theta_{j0}) + A_y \sin(\omega t + \phi_y) + R_j \sin(\omega t + \lambda) \end{aligned} \right\} \quad (3)$$

The geometry in Figure 4 can be related to Equation (1) by using the following relationship:

$$\xi = \pi - (\omega t + \lambda - \theta_j) \quad (4)$$

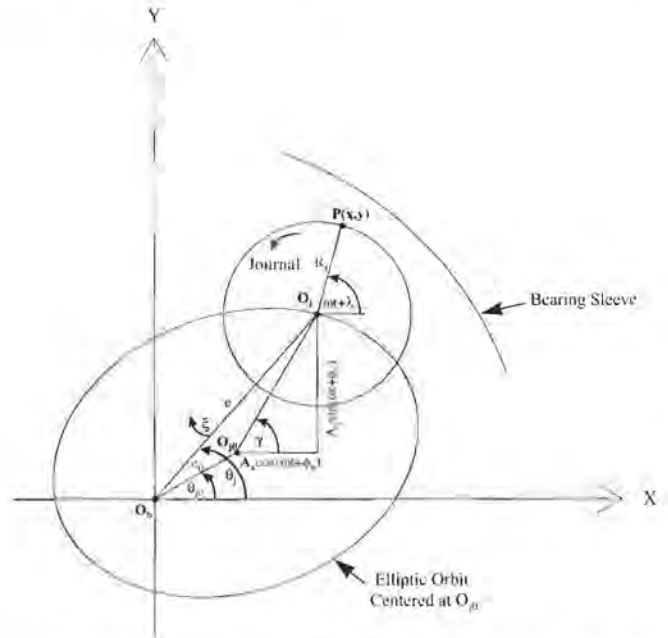


Figure 4. Schematic Diagram of Synchronous Orbit. (Courtesy Balbahadur and Kirk, 2002a)

where,

$$\theta_j = \tan^{-1} \left[ \frac{e_0 \sin(\theta_{j0}) + A_y \sin(\omega t + \phi_y)}{e_0 \cos(\theta_{j0}) + A_x \cos(\omega t + \phi_x)} \right] \quad (5)$$

The fourth step of the process requires that the hot spot and cold spot locations be determined. The detailed discussion about hot and cold spot locations will be given in the following sections. Assume the angle to define the location of hot spot,  $\lambda_0$ , is known. The time-dependent locations of the hot spot and the diametrically-opposite cold spot can now be obtained by using the following equations:

$$\left. \begin{aligned} x_H &= e_0 \cos(\theta_{j0}) + A_x \cos(\omega t + \phi_x) + R_j \cos(\omega t + \lambda_0) \\ y_H &= e_0 \sin(\theta_{j0}) + A_y \sin(\omega t + \phi_y) + R_j \sin(\omega t + \lambda_0) \end{aligned} \right\} \quad (6)$$

$$\left. \begin{aligned} x_C &= e_0 \cos(\theta_{j0}) + A_x \cos(\omega t + \phi_x) + R_j \cos(\omega t + \lambda_0 + \pi) \\ y_C &= e_0 \sin(\theta_{j0}) + A_y \sin(\omega t + \phi_y) + R_j \sin(\omega t + \lambda_0 + \pi) \end{aligned} \right\} \quad (7)$$

The parameters  $A_x$ ,  $A_y$ ,  $\phi_x$ , and  $\phi_y$  can be obtained directly from the forced response program in a rotordynamics software package that is currently used in both the classroom and industry (Kirk, et al., 1999).

The fifth step in the thermal instability analysis is to obtain the circumferential temperature distribution at the journal surface within the bearing. In order to obtain this temperature distribution, an energy equation must first be formulated and solved by considering a control box that encompasses the lubricant, journal, and bearing sleeve surfaces. Steady-state conditions and negligible axial heat flow are assumed for the analysis. The conservation of energy can generally be stated as: energy generation rate = energy outflux rate + energy accumulation rate. The steady-state assumption means that the accumulation rate is zero. Therefore, applying conservation of energy gives:

$$\dot{E}_{visc} = \left( \dot{E}_{lub} \Big|_{x+dx} - \dot{E}_{lub} \Big|_x + \dot{E}_j + \dot{E}_b \right) + 0 \quad (8)$$

where,  $\dot{E}_{visc}$  is the rate of viscous energy dissipation, which depends on the speed of the journal surface and the viscous shear stress.  $\dot{E}_{lub/s}$  and  $\dot{E}_{lub/s} dx$  represent rates of energy storage in and out of the control box.  $\dot{E}_j$  and  $\dot{E}_b$  are the rates of energy transferred to journal and bearing. Finally, the following equation can be derived (Balbahadur and Kirk, 2002a):

$$\frac{dT}{d\xi} + \frac{2H}{\rho_j c_j \omega h} T - \left( \frac{2HT_{amb}}{\rho_j c_j \omega h} + \frac{2\mu\omega R_j^2}{\rho_j c_j h^2} \right) = 0 \quad (9)$$

Equation (9) can be solved for the temperature distribution in either a plain journal bearing or in a tilting pad journal bearing.

The next step is to determine the thermally-induced bend in the overhung rotor. This bend can be represented as shown in Figure 5. The static bending moment  $M$  in the journal can be expressed as:

$$M = EI \frac{d\psi}{dz} \quad (10)$$

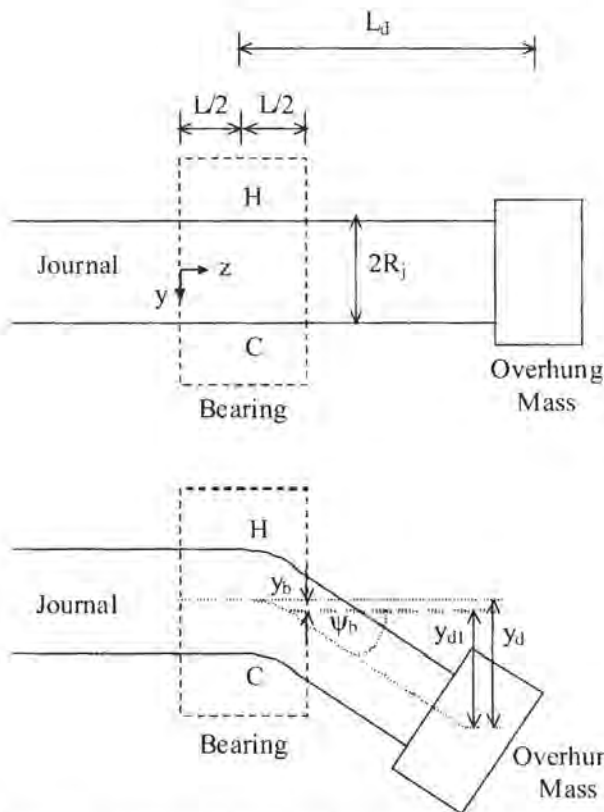


Figure 5. Thermally-Induced Bend in Rotor with Overhung Mass. (Courtesy Balbahadur and Kirk, 2002a)

where  $E$  = Young's modulus,  $I$  = area moment of inertia, and  $\psi$  = bend angle as shown in Figure 5.

The maximum stress in the shaft can be written as:

$$\sigma_{max} = \frac{R_j M}{I} \quad (11)$$

If this maximum stress is primarily caused by thermal effects, then:

$$\sigma_{max} = E\alpha\Delta T \quad (12)$$

where  $\alpha$  = thermal conductivity of the journal,  $\Delta T$  is the overall mean temperature difference between the hot and the cold spots. It is assumed that  $\Delta T$  is independent of axial position within the

bearing. Furthermore, the small deflections allow the thermal and mechanical problems to be uncoupled.

From Equations (10), (11), and (12), the following equation can be obtained:

$$\frac{d\psi}{dz} = \frac{\alpha\Delta T}{R_j} \quad (13)$$

For a given journal speed and orbit, the right-hand side of Equation (13) is essentially constant. Therefore, Equation (13) can be integrated between the start of the bearing, where it is assumed that the bend angle is zero, and some arbitrary axial distance,  $z$  (refer to Figure 5), to give:

$$\psi = \frac{dy}{dz} = \frac{\alpha\Delta T}{R_j} z \quad (14)$$

where  $y$  = deflection of the journal. Equation (14) can be evaluated at the end of the bearing to give the bend angle at that location:

$$\psi_b = \frac{\alpha\Delta T}{R_j} L \quad (15)$$

Also, Equation (14) can be integrated over the bearing to give the deflection at the end of the bearing:

$$y_b = \frac{1}{2} \frac{\alpha\Delta T}{R_j} L^2 \quad (16)$$

The additional deflection at the overhung mass location can then be calculated using the small angle assumption:

$$y_d = \left( L_d - \frac{L}{2} \right) \sin(\psi_b) \approx \left( L_d - \frac{L}{2} \right) \psi_b \quad (17)$$

By substituting Equation (15) into (17) and adding Equations (16) and (17), the total thermal deflection at the overhang can be expressed as follows:

$$y_d = \frac{\alpha\Delta T}{R_j} LL_d \quad (18)$$

Equation (18) gives the thermal deflection of the overhung mass. This deflection can be converted into a thermal imbalance:

$$U_t = m_d y_d \quad (19)$$

where  $m_d$  = overhung mass.

The proposed solution method requires the calculation of the bearing journal response for an initial mechanical imbalance. A nominal initial mechanical imbalance,  $U_m$ , has been defined as the imbalance created from a centrifugal force equal to 10 percent of the total static rotor weight.  $U_m$  will be calculated for the rotor running at its maximum continuous operating speed,  $\omega_{MCO}$ , which can be mathematically defined as:

$$U_m = \frac{0.1W}{\omega_{MCO}^2} \quad (20)$$

This imbalance will be assumed to act at an angle of zero degrees with respect to a coordinate system on the rotor, and will be located at the center-of-gravity of the overhung mass.

The resultant imbalance  $U$  from  $U_m$  and  $U_t$  can be represented as shown in Figure 6. For step seven of the analysis, the mechanical and thermal imbalances can be combined to produce the resultant imbalance, which can be represented as follows:

$$U = \sqrt{U_t^2 + U_m^2 - 2U_t U_m \cos(\alpha t - \theta_{CH})} \quad (21)$$

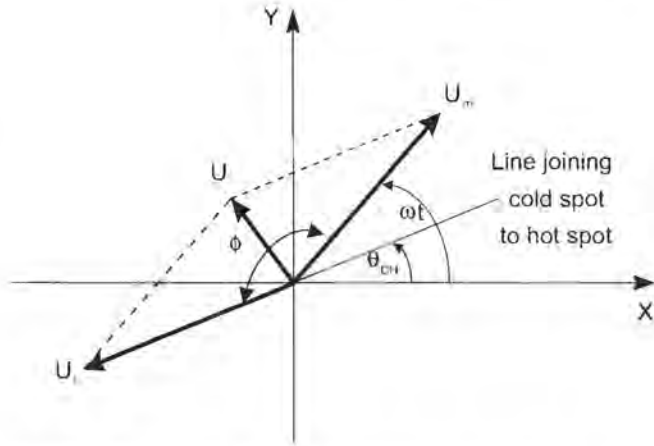


Figure 6. Mechanical, Thermal, and Resultant Unbalances.

The angle  $(\omega t - \theta_{chi})$  is actually calculated by averaging similar angles at several different dynamic points in the synchronous orbit. Then the phase angle,  $\phi$ , between thermal and mechanical imbalances can also be obtained.

To complete the system analysis, the eighth and final step requires that a threshold imbalance,  $U_{thr}$ , be defined. This total imbalance is assumed to be 50 percent larger than the original mechanical imbalance. Hence, the threshold imbalance force is equal to 15 percent of the rotor weight and can be mathematically expressed as:

$$U_{thr} = \frac{0.15W}{\omega^2} \quad (22)$$

where  $W$  = rotor weight and  $\omega$  = variable angular journal speed.

The rotor is considered to be unstable whenever  $U$  exceeds  $U_{thr}$ . As a result, the threshold speed for instability,  $\omega_{thr}$ , occurs when  $U = U_{thr}$ . This instability criterion can be obtained graphically from the intersection of the  $U - \omega$  and the  $U_{thr} - \omega$  curves and it determines the onset of the Morton effect in the rotor system.

Based on the model presented above, a Morton analysis software program was developed. A summary of the results obtained by application of this program to selected machines discussed in the literature will be presented in the following section of this paper. In addition, a typical overhung pipeline compressor application will be discussed to illustrate the type of machine likely to require evaluation and correction for thermal instability.

**KEOGH AND MORTON CASE**

Keogh and Morton (1994) conducted a theoretical analysis on a symmetric rotor, as illustrated in Figure 7. This rotor consists of a shaft with a step variation in diameter and it is supported by two identical plain journal bearings. On either shaft end, there is a disk with constant mass at an overhung position.

Keogh and Morton examined the stability of this rotor by calculating the eigenvalues of the rotor system and determining the corresponding growth factors. The positive growth factor would indicate a theoretical instability. Their growth factor plot revealed that the critical speed range, in which rotor thermal bending can occur, is between 1023 rad/s (9769 rpm) and 1086 rad/s (10,371 rpm).

Table 1 provides the data necessary for simulating the Keogh and Morton rotor. The simulation software program and the Morton analysis software program were used to predict a synchronous thermal instability range from 1047 rad/s (10,001 rpm) to 1206 rad/s (11,521 rpm). This predicted instability range overlaps the Keogh and Morton calculated instability range.

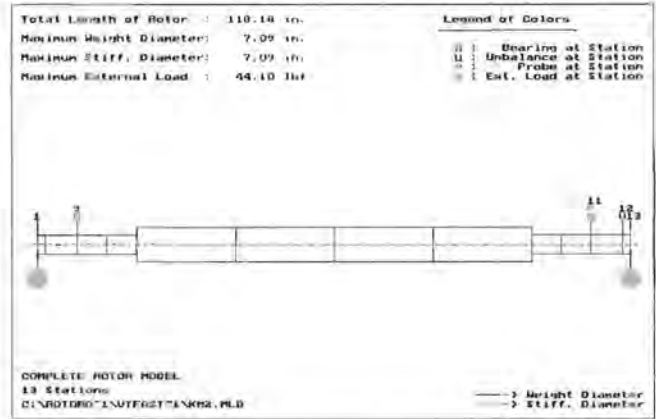


Figure 7. Computer Model of Keogh and Morton Symmetric Rotor.

Table 1. Data for Keogh and Morton Rotor.

Parameter	SI Units	EG Units
<b>Lubricant Properties</b>		
Density $\rho_l$	850 kg/m <sup>3</sup>	0.031 lbm/in. <sup>3</sup>
Specific heat capacity $c_l$	2000 J/kg/°C	0.478 Btu/lbm/°F
Supply temperature $T_{in}$	45.0 °C	113 °F
Supply viscosity $\mu_0$	0.0095 Pa s	1.38 µreyn
Thermovisc. coeff. $\beta$	0.029 °C <sup>-1</sup>	0.016 °F <sup>-1</sup>
<b>Bearing Properties</b>		
Length $L$	0.035 m	1.38 in
Radial clearance $C_r$	1.00E-04 m	3.94 mils
Heat transfer $H$	50 W/m <sup>2</sup> /°C	2.43E-5 hp/in. <sup>2</sup> /°F
Bearing load $W_b$	2500 N	562 lbf
Journal radius $R_j$	0.050 m	1.97 in
Journal C.T.E $\alpha$	1.10E-05 °C <sup>-1</sup>	6.11E-06 °F <sup>-1</sup>
<b>Rotor Properties</b>		
Rotor weight $W$	5000 N	1124 lb <sub>f</sub>
Overhung mass $m_d$	32.3 kg	71.3 lb <sub>m</sub>
Overhung Distance $L_o$	0.16 m	6.4 in
Max. Cont. Op. $\omega_{max}$	1047 rad/s	10000 RPM
Init. Mech. Imbalance $U_m$	4.54E-4 kg m	0.63 oz in

**Hot Spot Location**

Two methods to locate the hot and cold spot positions have been examined. They are referred to as the original and improved method. The following discussion will detail the difference between the two methods.

**Original Method**

In this method, the hot spot ( $H$ ) will be defined as the point closest to the bearing sleeve at time  $t = 0$ . In this configuration, it is also assumed that  $\gamma = \omega t + \lambda$  so that  $O_{j0}$ ,  $O_j$ , and  $P = H$  all lie on the same straight line (refer to Figures 4 and 8). Hence, at time  $t = 0$ :

$$\gamma = \gamma_0 = \tan^{-1} \left( \frac{A_y \sin \phi_y}{A_x \cos \phi_x} \right) = \lambda_0 \quad (23)$$

**Improved Method**

For a plain journal bearing, the hot spot can be defined as the point closest to the bearing at some moment  $t = t_m$ . On the bearing dynamic orbit, there exists a point that has the maximum dynamic eccentricity. The time corresponding to this dynamic position can be obtained:

$$t_m = t_{e_{max}} \quad (24)$$

Assume at this dynamic position that the bearing has the hot spot with the minimum film thickness. In this configuration, the hot

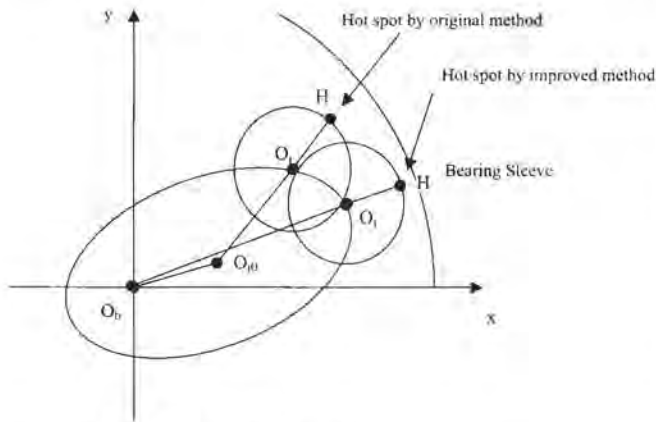


Figure 8. Schematic for Hot Spot Orientation.

spot  $H$  is located on the straight line with  $O_h$  and  $O_j$  (Figure 8). The following equation can be obtained:

$$\omega t_m + \lambda_0 = \tan^{-1} \left( \frac{e_0 \sin \theta_{j0} + A_y \sin(\omega t_m + \phi_y)}{e_0 \cos \theta_{j0} + A_x \cos(\omega t_m + \phi_x)} \right) \quad (25)$$

The angle to define the hot spot,  $\lambda_0$ , can be determined from Equation (25).

In addition, to make the dynamic position with maximum dynamic eccentricity match with the positions used in codes to calculate the average temperature difference, the orientation of all dynamic positions including the first dynamic position at  $t = 0$  should be adjusted according to the resultant time lag.

The advantage of the improved method is that it ensures the hot spot it finds is the "real" hot spot, which means the temperature difference at this dynamic point should be the maximum one among the entire dynamic points. This has been proved in the calculation of the plain journal bearing cases.

For the Keogh and Morton rotor, an imbalance response analysis revealed that the rotor has a critical speed (fourth critical) near 10,500 rpm. This lateral critical speed creates large amplitude orbits in this region. One such orbit (at 10,505 rpm) is illustrated in Figures 9 and 10.

The lower left and the upper right corners of this orbit show that, in these regions, the rotor is running very close to the radial bearing clearance,  $C_b$ . This configuration implies that the film thickness at the hot spot (in symbol  $x$ ) would be very low, while the diametrically-opposite cold spot (in symbol  $o$ ) would experience higher film thickness values. Since a lower film thickness is associated with higher viscous dissipation and higher temperatures, a strong thermal gradient will develop across the journal. Such a gradient will cause the  $\Delta T$  value to be high and promote a thermal instability.

On the other hand, lower amplitude orbits, which are further away from the critical speed, keep the rotor away from the clearance circle and are less likely to be associated with high  $\Delta T$  values. Hence, the orbit as shown in Figures 11 and 12 would not give rise to a thermal bending instability. The lower speed of the 5730 rpm orbit also reduces the amount of viscous dissipation, and this further stabilizes this orbit relative to the 10,505 rpm one.

Figures 9, 10, 11, and 12 also show the comparison of the orbit plots calculated by two methods, at 5730 rpm and 10,505 rpm, respectively. It can be seen that the maximum temperature differences at 10,505 rpm are 140.67°F (original) and 148.53°F (improved), respectively. Although the maximum temperature difference at 5730 rpm has the same value (25.91°F) by the two methods (unique in all calculated speeds), the average  $\Delta T$  by the improved method is still slightly larger than that by the original method.

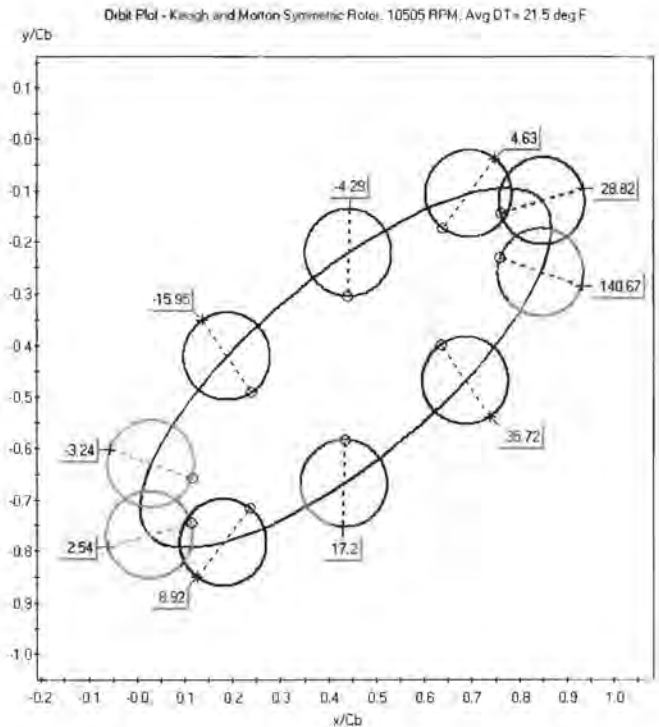


Figure 9. Orbit Plot by Original Method, 10,505 RPM.

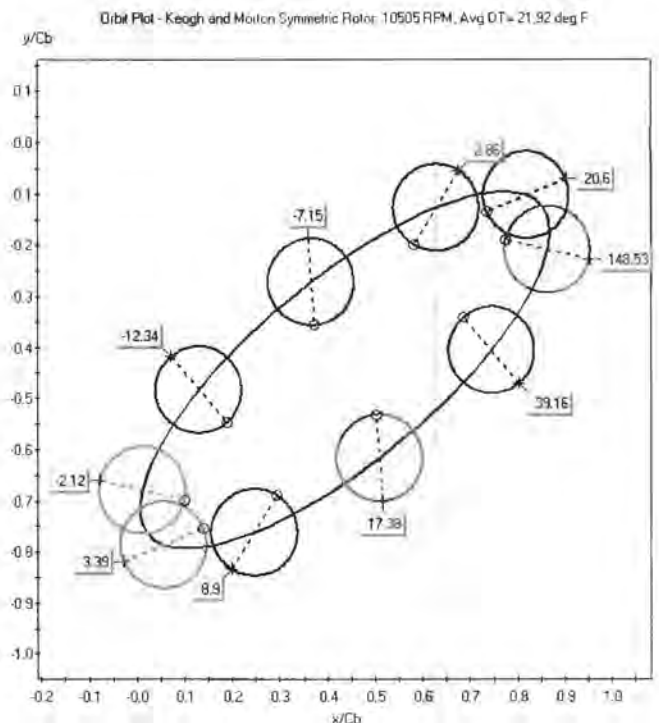


Figure 10. Orbit Plot by Improved Method, 10,505 RPM.

Figures 13 and 14 are the stability plots of the Keogh and Morton rotor calculated by two methods, respectively. The resultant unbalance curve is obtained by employing the not-a-knot spline method to fit the results on the calculated speeds. The instability thresholds are obtained from the intersection of the resultant unbalance and threshold unbalance curves. From the results given in Figures 13 and 14, there is an instability threshold at a speed of 10,038 rpm by the improved method (10,031 rpm,

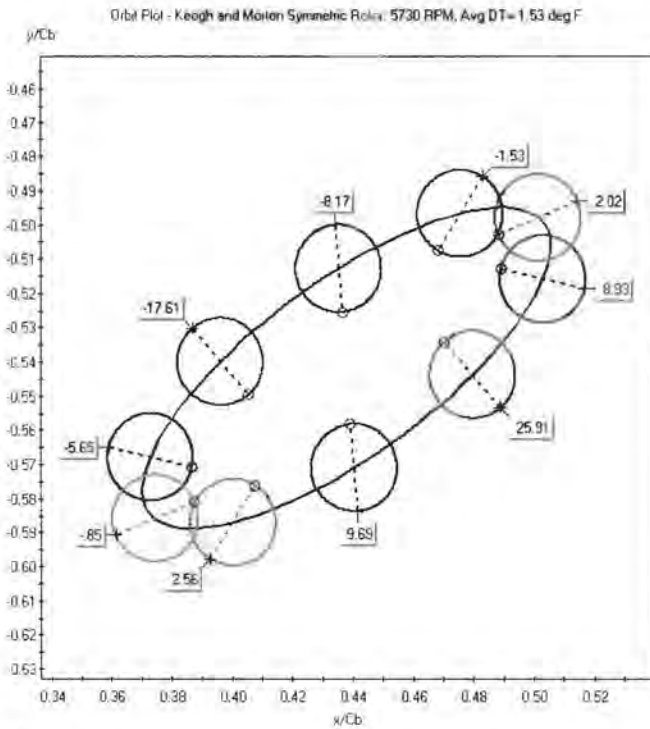


Figure 11. Orbit Plot by Original Method, 5730 RPM.

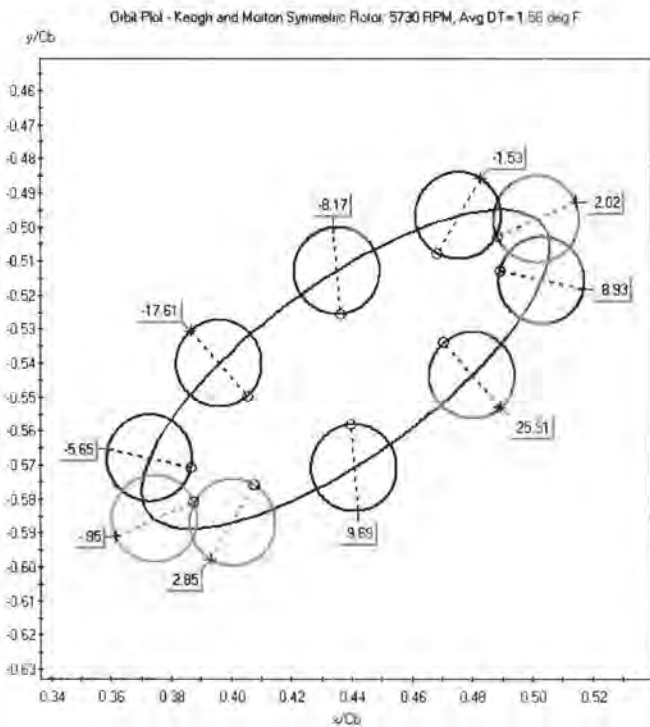


Figure 12. Orbit Plot by Improved Method, 5730 RPM.

by the original method), which is between the lower and upper-speed limits Keogh and Morton indicated. In addition, the stability plot indicates another range of instability after 12,292 rpm by the improved method (12,285 rpm, by the original method). The instability results by the two methods are very close (percentage difference < 0.07 percent). The improved method is considered to be a better solution and will be used in the following analysis.

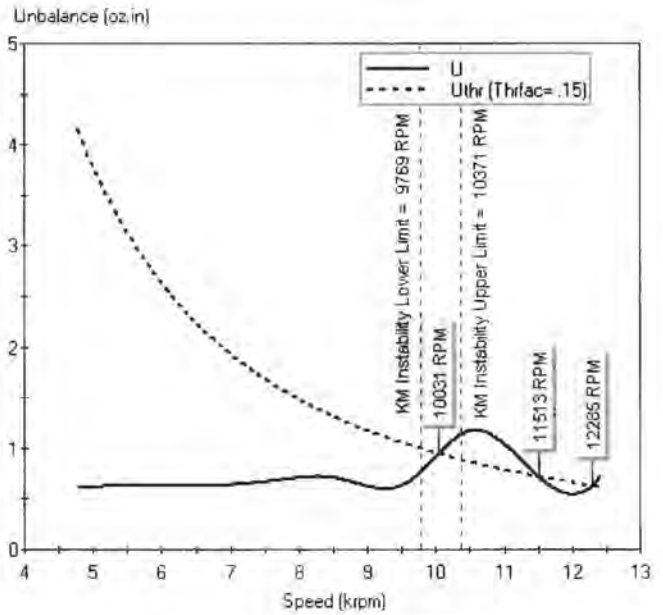


Figure 13. Stability Plot of Keogh and Morton Rotor by Original Method.

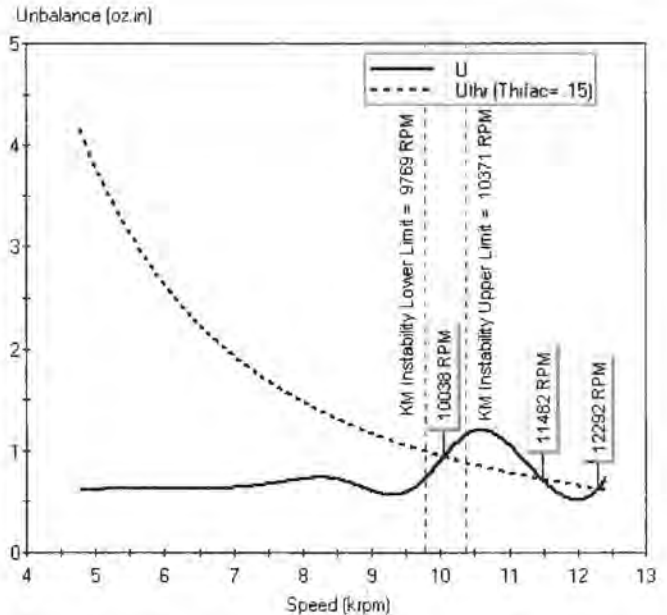


Figure 14. Stability Plot of Keogh and Morton Rotor by Improved Method.

Average Temperature Difference

The previous analysis used 10 dynamic points to calculate the average temperature differences  $\Delta T$ . In general, more dynamic points will contribute to the calculation accuracy. In order to examine the effect of the number of dynamic points on the results, two other situations have been calculated. Figures 15, 16, 17, and 18 are the orbit plots by adopting 5 and 20 dynamic points, respectively. Figures 19 and 20 show the corresponding stability plots.

At a speed of 5730 rpm, the percentage difference for the average temperature difference  $\Delta T$  by using 5 and 20 dynamic points relative to that by 10 points is 117.3 percent and -13.5 percent, respectively. At a speed of 10,505 rpm, the difference is 45.8 percent (5 points) and 12.6 percent (20 points), respectively.

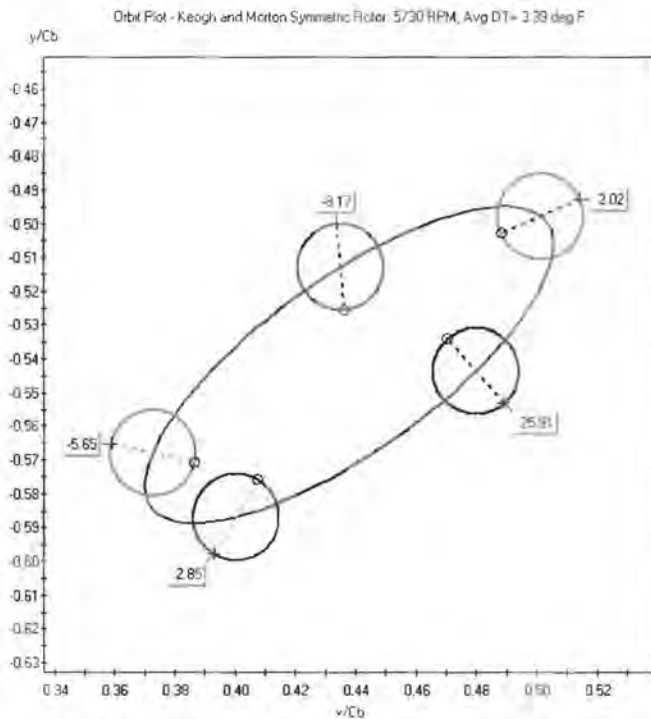


Figure 15. Orbit Plot with 5 Dynamic Points, 5730 RPM.

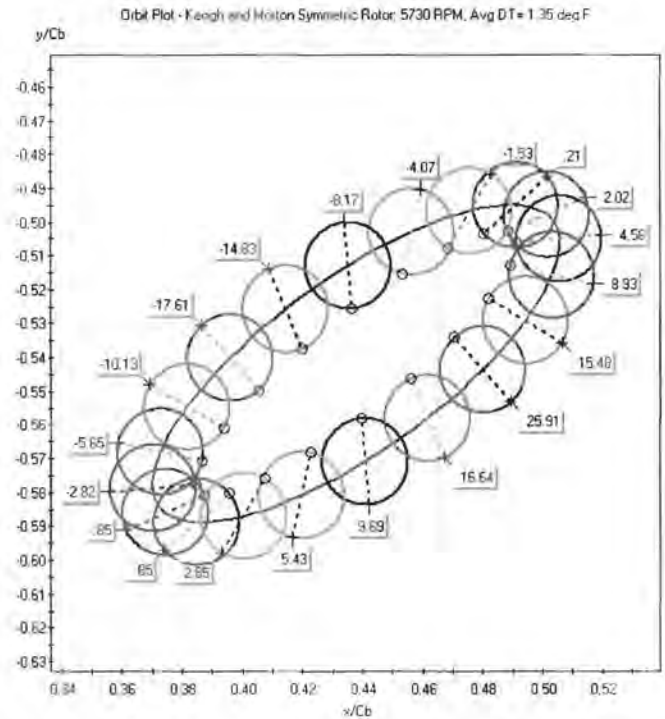


Figure 17. Orbit Plot with 20 Dynamic Points, 5730 RPM.

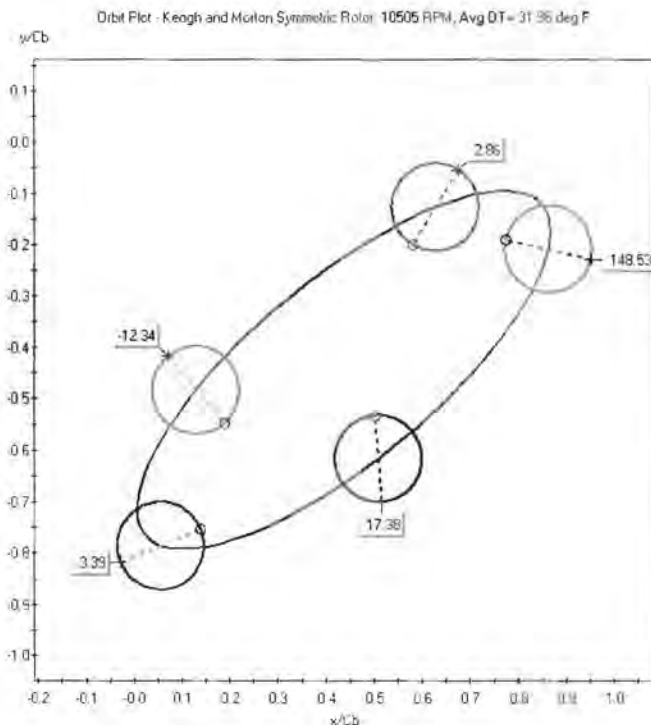


Figure 16. Orbit Plot with 5 Dynamic Points, 10,505 RPM.

More important, the percentage difference for instability speed by using 5 and 20 dynamic points relative to that by 10 points is -1.06 percent and 0.46 percent. It can be seen that when the number of dynamic points is increased to 10 or more, the results appear to be acceptable regarding the needed accuracy for this stability evaluation. Therefore, the discussion in this paper uses 10 as the number of dynamic points for average temperature difference calculation.

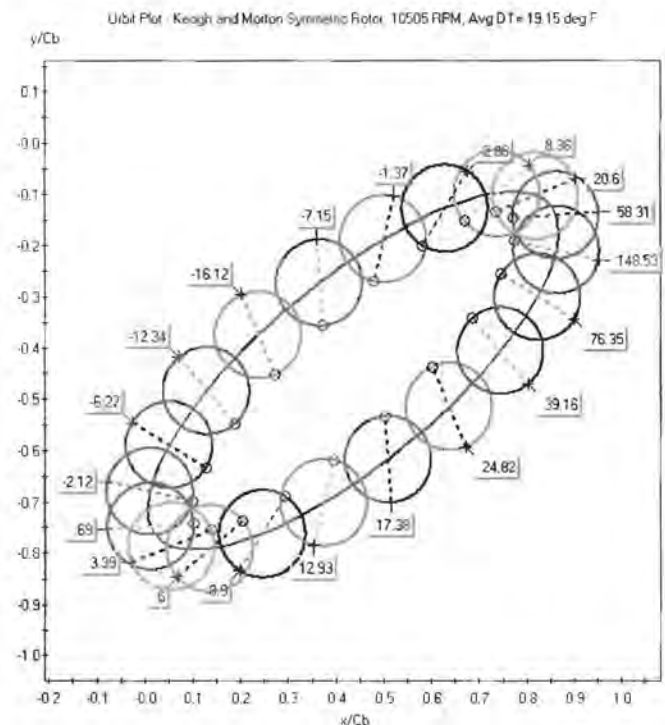


Figure 18. Orbit Plot with 20 Dynamic Points, 10,505 RPM.

### FAULKNER, STRONG, AND KIRK CASE

Faulkner, Strong, and Kirk (1997a, 1997b) did an experimental study of a large turbocharger. The analytical model of this rotor is shown in Figure 21. The turbocharger had a centrifugal compressor impeller at one end and a radial inflow turbine disk at the other end. This machine was supported by two three-axial-groove journal bearings that consist of a plain journal bearing with three small grooves cut along the bearing length. For simplicity, this type

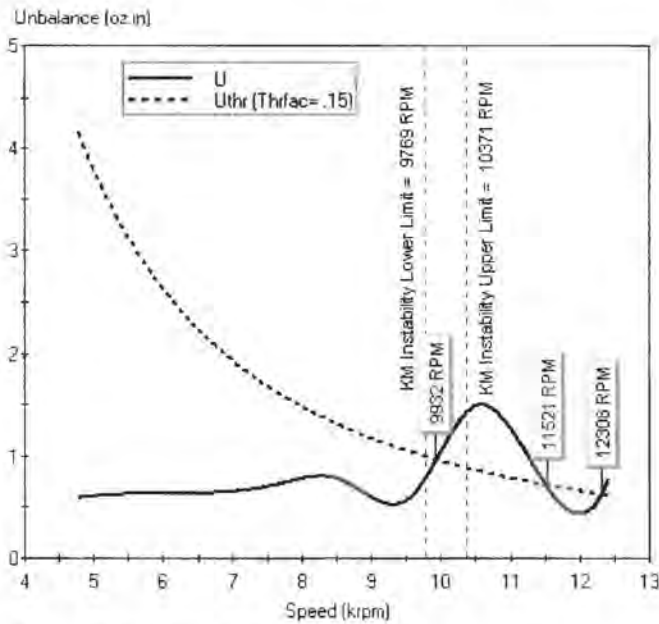


Figure 19. Stability Plot by 5 Dynamic Points.

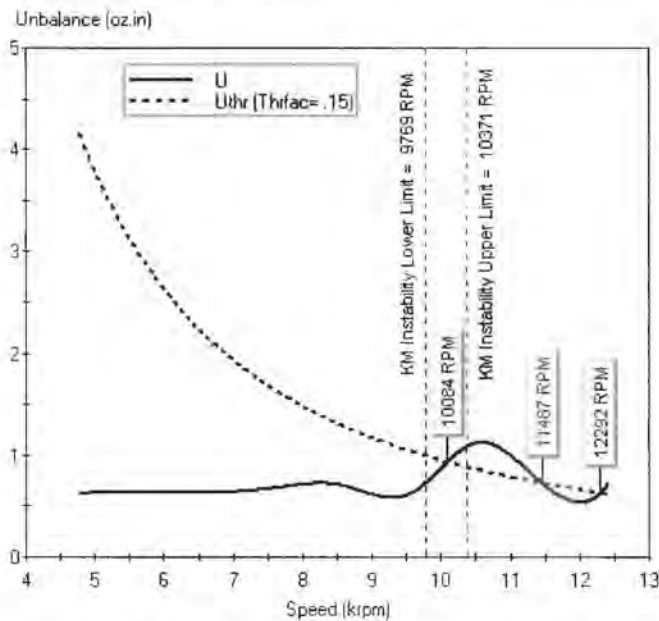


Figure 20. Stability Plot by 20 Dynamic Points.

of bearing will be approximated as a plain journal bearing. Other relevant information on the turbine end of this turbocharger is shown in Table 2.

If the heat transfer coefficient is not known (as is the case with the turbocharger bearings), a default value can be calculated by using the following formula:

$$H = (0.5)(25.5)(\omega R_j)^{0.7} (\mu_0)^{-0.2} (2\pi R_j)^{-0.4} \quad (26)$$

Equation (26) is based on an expression that was derived for tilting pad journal bearings (Ettles, 1992).

During operation, it was observed that the turbocharger became unstable near 9900 rpm. Faulkner, Strong, and Kirk initially thought that the instability was due to the turbine wheel becoming loose at the high operation speeds. However, a careful inspection of the turbine wheel position, before and after operation, indicated

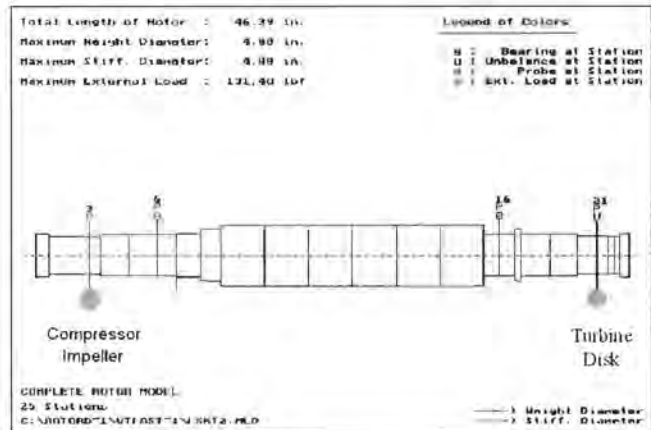


Figure 21. Computer Model of Faulkner, Strong, and Kirk Turbocharger Rotor.

Table 2. Data for Faulkner, Strong, and Kirk Turbocharger Rotor.

Parameter	SI Units	EG Units
<b>Lubricant Properties</b>		
Density	$\rho_l$ 850 kg/m <sup>3</sup>	0.031 lbm/in <sup>3</sup>
Specific heat capacity	$c_l$ 2000 J/kg°C	0.478 Btu/lbm°F
Supply temperature	$T_{li}$ 87.8 °C	190 °F
Supply viscosity	$\mu_0$ 0.0066 Pa s	0.952 µreyn
Thermovisc. coeff.	$\beta$ 0.031 °C <sup>-1</sup>	0.017 °F <sup>-1</sup>
<b>Bearing Properties</b>		
Length	$L_b$ 0.057 m	2.24 in
Radial clearance	$C_r$ 7.11e-5 m	2.8 mils
Heat transfer coefficient	$H$ default W/m <sup>2</sup> °C	default hp/in <sup>2</sup> °F
Bearing load	$W_b$ 916 N	206 lbf
Journal radius	$R_j$ 0.041 m	1.63 in
Journal C.T.E	$\alpha$ 1.10E-05 °C <sup>-1</sup>	6.11E-06 °F <sup>-1</sup>
<b>Rotor Properties</b>		
Rotor weight	$W$ 1877 N	422 lb <sub>f</sub>
Overhung mass	$m_d$ 61.7 kg	136 lb <sub>m</sub>
Overhang Distance	$L_d$ 0.20 m	7.71 in
Max. Cont. Op. Speed	$\omega_{SCOS}$ 1047 rad/s	10000 RPM
Initial Mech. Imbalance	$U_m$ 1.73e-4 kg m	0.24 oz in

that the wheel did not move while the turbocharger was running. Furthermore, a damped critical speed analysis failed to justify the existence of a lateral critical speed near 9900 rpm. It was finally concluded that the source of the instability was the thermal bowing of the rotor shaft near the turbine end of the turbocharger.

After using the current thermal instability model to analyze the turbocharger, it was found that the thermal instability was predicted to occur around 9590 rpm near the turbine end of the turbocharger (Figure 22). Unlike the Keogh and Morton case, the turbocharger does not encounter critical speeds with low damping in the given speed range. As a result, there are no large amplitude orbits to produce a sudden instability hump. The monotonic increase in  $U$  can be explained by the increase in speed that leads to increased viscous dissipation, higher  $\Delta T$  values, and more incentive for thermal bending. Figures 23, 24, and 25 illustrate this trend of higher speed leading to higher  $\Delta T$  values. The figures also show that the orbits become more centered at higher speeds, i.e., the center of the elliptical orbit approaches the bearing center ( $x/C_b = 0, y/C_b = 0$ ) as the rotor speed increases. A more centered orbit means that the hot spot and the cold spot experience almost constant film thickness values, and such a configuration causes a relatively steady thermal gradient to develop. In fact, this gradient would be the most steady when the orbit is a circle that is completely centered.

For this case, the increase of speed mainly contributes to the increased  $\Delta T$  values (refer to Figures 23, 24, and 25). The higher  $\Delta T$  values normally mean the larger thermal unbalance. However,

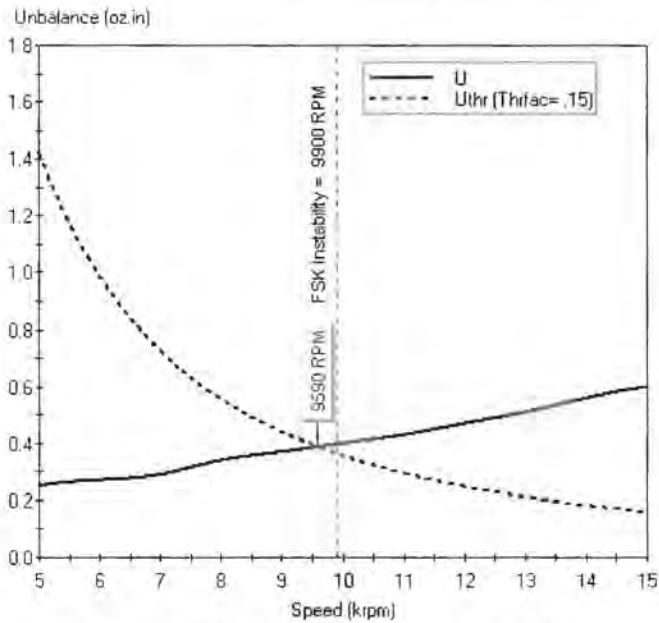


Figure 22. Stability Plot for Faulkner, Strong, and Kirk Rotor.

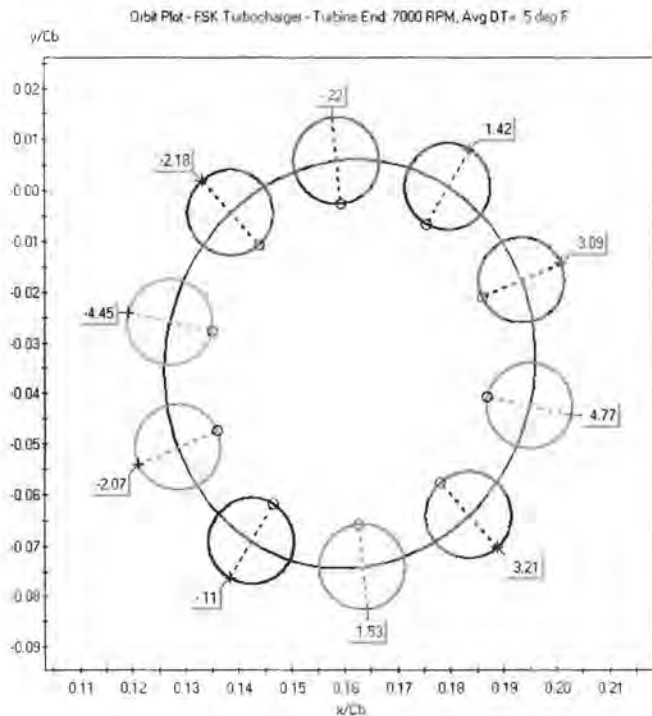


Figure 23. Orbit Plot at 7000 RPM.

it is not the only factor leading to the unstable operation after 9590 rpm. Another key element is the phase angle between the mechanical imbalance and thermal imbalance. The magnitude of phase angle between  $U_i$  and  $U_m$  will affect the value of resultant imbalance (refer to Figure 6). A larger phase angle around 180 degrees would lead the thermal bending to balance the mechanical imbalance, which is definitely beneficial to the stability. The small phase angle would produce large values of resultant imbalance. It is a worse situation as far as thermal stability is concerned. In Figures 23, 24, and 25, the first dynamic point ( $t \approx 0$ ) is shown as  $-1.11$ ,  $-2.21$ , and  $-6.72$ , respectively. The direction of thermal imbalance can be recognized from hot spot to cold spot, while the mechanical imbalance is defined at an angle of zero degrees with

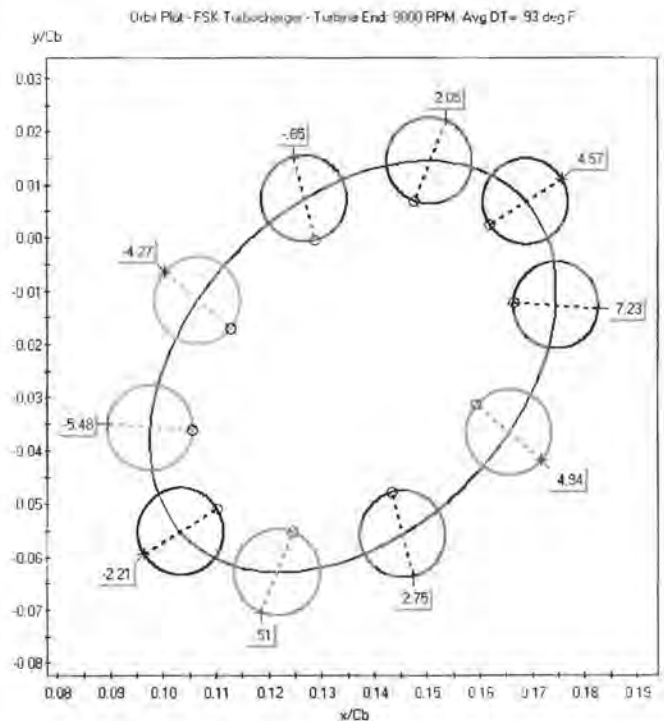


Figure 24. Orbit Plot at 9000 RPM.

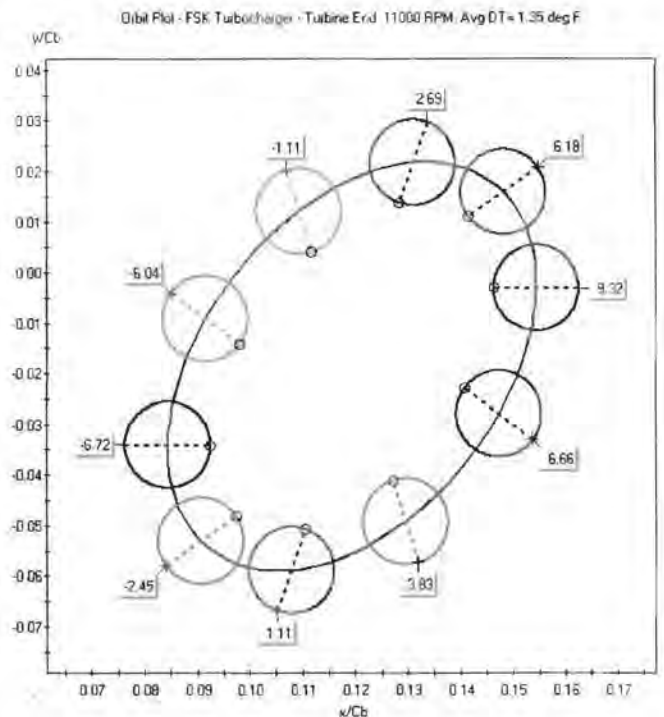


Figure 25. Orbit Plot at 11,000 RPM.

respect to a coordinate system on the rotor. It can be seen clearly that the phase angle between  $U_i$  and  $U_m$  steadily decreases with the increase of speed. At a speed of 11,000 rpm, this phase angle approaches zero, which leads to the almost direct addition of thermal and mechanical imbalances.

It was previously found in the Keogh and Morton case study by Balbahadur and Kirk (2002b) that the larger amplitudes of the rotor will lead to higher  $\Delta T$  values and larger thermal imbalance. Meanwhile, centered, circular orbit also contributes to higher tem-

perature difference values. These results indicate the worst scenario for the Morton effect as follows: centered, circular, large amplitude orbit at high speed range, and small phase angle between thermal and mechanical imbalances.

TILTING PAD JOURNAL BEARING CASE STUDIES

A more recent case for discussion came from a domestic compressor company. A compressor rerate was unstable on the test stand and it was thought it might be a thermal instability. The lead author's university was contacted to evaluate the rotor for thermal instability using the newly developed analysis. The rotordynamics software program's rotor model for the compressor is shown in Figure 26.

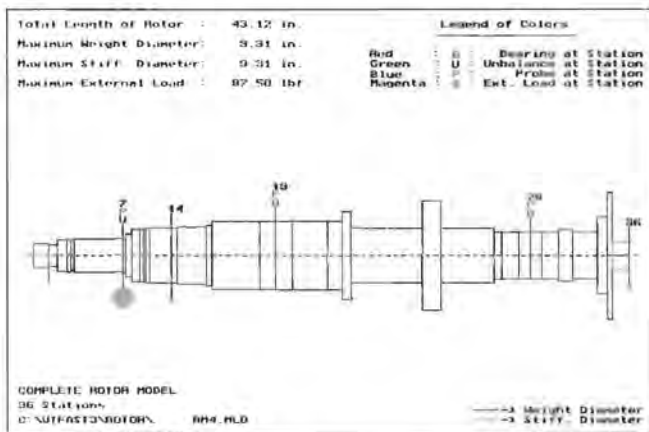


Figure 26. Computer Model of Pipeline Compressor Rotor.

The required data for thermal stability analysis is presented in Table 3 for the pipeline compressor. The calculated speed range is from 6000 to 11,000 rpm. Figure 27 shows the temperature, pressure, and film thickness distributions at 8000 rpm, obtained from the Morton analysis software program's internal bearing analysis.

Table 3. Data for Pipeline Compressor Rotor, L/D = 0.476.

PARAMETER	SI Units	EG Units
<b>Pad Parameters</b>		
$N_p$ Number of Pads	5	5
$l_p$ Axial pad or brg length	0.0604 m	2.38 in.
$t_p$ Pad thickness	0.0127 m	0.5 in.
$C_{rp}$ Radial pad clearance	133.35 $\mu$ m	5.25 mils
$\alpha_p$ Angular dimension of pad	56 deg	56 deg
$\beta_p$ Pivot angles of pads (deg)	18, 90, 162, 234, 306	18, 90, 162, 234, 306
$m$ Preload factor	0.34	0.34
$f_p$ Frac. ang. position of pivot	0.5	0.5
<b>Journal/Bearing Parameters</b>		
$R_j$ Radius of journal	0.0635 m	2.50 in.
$C_r$ Radial Bearing clearance	88.14 $\mu$ m	3.47 mils
$W_b$ Bearing load	1277 N	287 lbf
$M_o$ Overhang Mass	77.45 kg	170.4 lb <sub>m</sub>
$L_p$ Overhang Distance	0.227 m	8.95 in.
$W_r$ Rotor Weight	1202 N	270 lbf
$U_{or}$ Initial Mecht. Imbalance	0.11 kg mm	0.15 oz in.
<b>Lubricant Parameters</b>		
$P_s$ Lubricant supply pressure	0.104 MPa	15 psi
$T_s$ Lubricant supply temp.	50 °C	122 °F
$\beta$ Thermoviscosity index	0.031 /°C	0.017 /°F
$\mu_s$ Lubricant supply viscosity	20.3 cP	2.94 greyn
$\rho_l$ Lubricant density	888 kg/m <sup>3</sup>	0.031 lb <sub>m</sub> /in <sup>3</sup>
$c_l$ Lubricant sp. heat capacity	1992 J/kg/K	0.478 Btu/lb <sub>m</sub> /°F

The two methods for locating the hot spot discussed before can still be used in tilting pad journal bearing calculations. The following analysis employed the improved method. The stability plot is shown in Figure 28. It can be seen that thermal instability is predicted to occur at 9895 rpm. From the test stand operation, the instability was reported at a speed of 10,200 rpm.

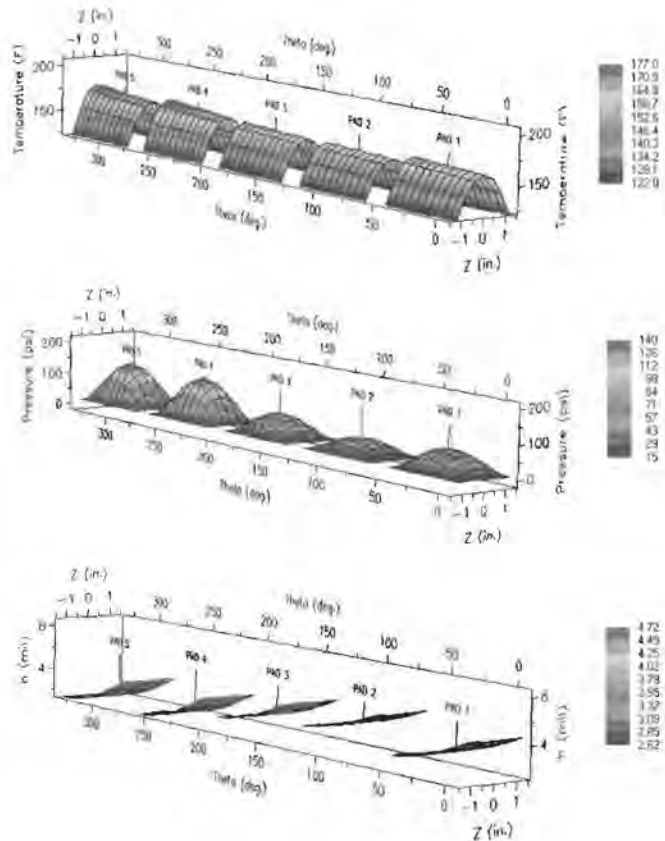


Figure 27. Temperature, Pressure, and Film Thickness at 8000 RPM, L/D = 0.476.

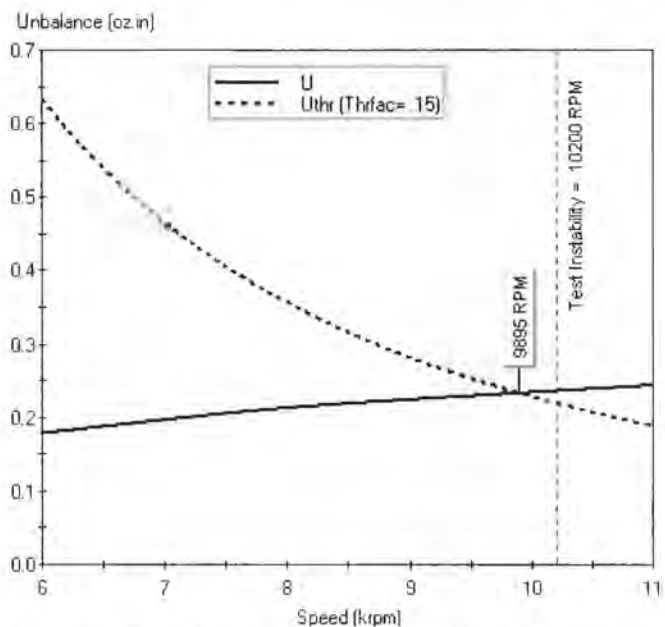


Figure 28. Stability Plot for Pipeline Compressor Rotor, L/D = 0.476.

Figures 29, 30, and 31 are the orbit plots at 6000 rpm, 8000 rpm, and 10,000 rpm, respectively. It can be seen that the phase angle between thermal and mechanical imbalances gradually decreases with the increase of speed. This mechanism, in addition to the increased thermal imbalance, eventually leads to the thermal instability.

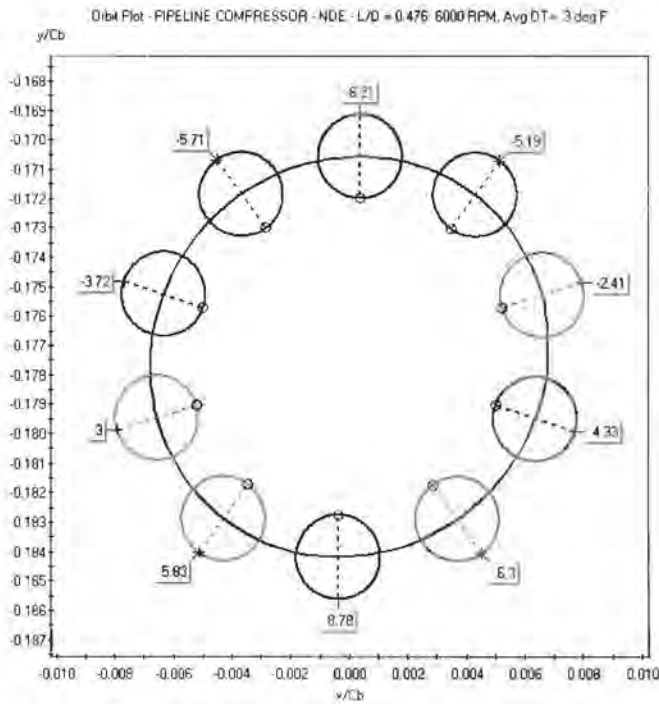


Figure 29. Orbit Plot of Pipeline Compressor Rotor at 6000 RPM,  $L/D = 0.476$ .

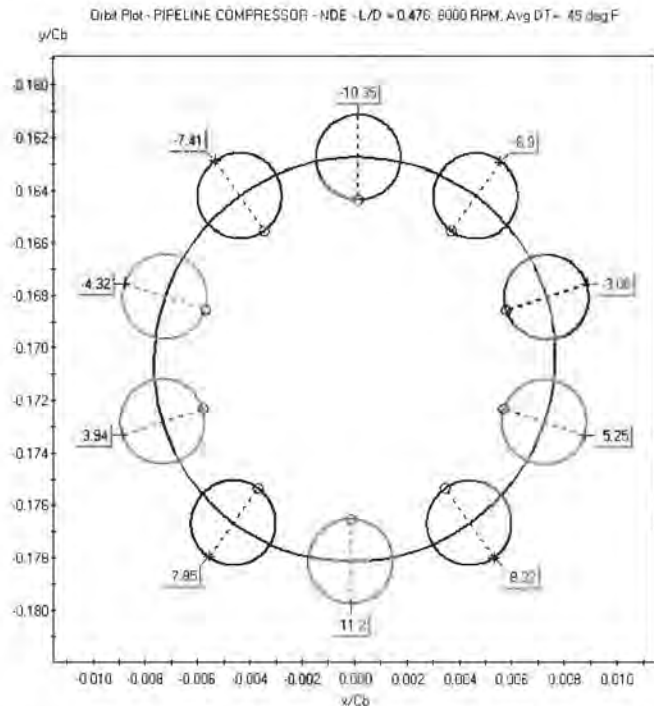


Figure 30. Orbit Plot of Pipeline Compressor Rotor at 8000 RPM,  $L/D = 0.476$ .

The elimination of the thermal instability may be achieved by any procedure that will sufficiently reduce the thermal gradient in the journal area of the rotor shaft. A simple remedy that was proven on the Faulkner turbocharger, was to load the bearing to a higher eccentricity ratio by reducing the load capacity of the bearing. For fixed geometry bearings, this is a simple procedure. For tilting pad bearings, a modification in pad length may be an acceptable solution. To prove this in the Morton software analysis, consider the design as shown in Table 4, where the  $L/D$  has been reduced

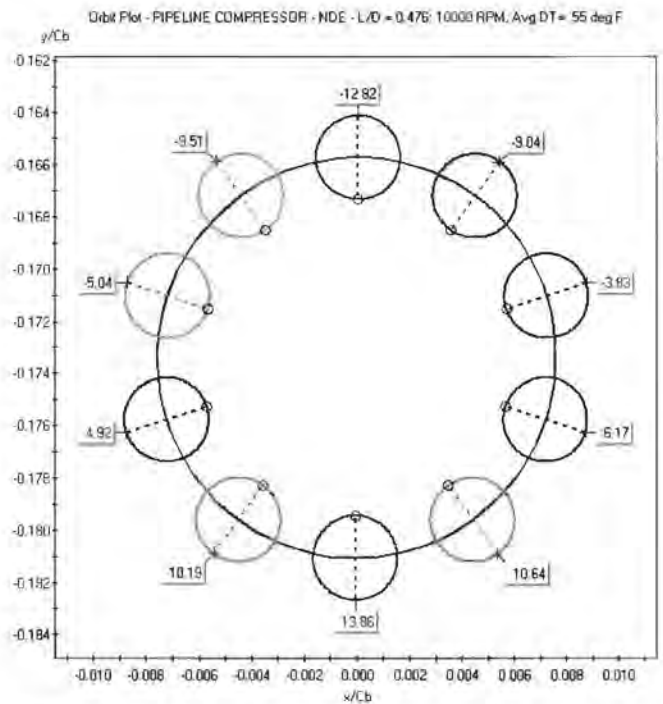


Figure 31. Orbit Plot of Pipeline Compressor Rotor at 10,000 RPM,  $L/D = 0.476$ .

from 0.476 to 0.25. The resulting stability prediction indicates the threshold has moved up to 10,675 rpm (refer to Figures 32, 33, 34, 35, and 36). The compressor on test had the bearing length reduced and the instability was, in fact, eliminated. Hence, the new analysis is in agreement with the test stand result. However, the threshold speed is still close to the desired operating speed and proper balance will be essential for continued stability.

Table 4. Data for Pipeline Compressor Rotor, Reduced Width Pads,  $L/D = 0.25$ .

PARAMETER	SI Units	EG Units
<i>Pad Parameters</i>		
$N_p$ Number of Pads	5	5
$L_p$ Axial pad or brg length	0.032 in	1.25 in.
$t_p$ Pad thickness	0.030 in	1.20 in.
$C_p$ Radial pad clearance	177.8 $\mu$ m	7 mils
$\Delta_p$ Angular dimension of pad	56 deg	56 deg
$\theta_p$ Pivot angles of pads (deg)	18, 90, 162, 234, 306	18, 90, 162, 234, 306
$m$ Preload factor	0.5	0.5
$f_p$ Frac. ang. position of pivot	0.5	0.5
<i>Journal/Bearing Parameters</i>		
$R_j$ Radius of journal	0.0635 in	2.50 in.
$C_b$ Radial Bearing clearance	88.9 $\mu$ m	3.5 mils
$W_b$ Bearing load	1277 N	287 lbf
$M_d$ Overhang Mass	77.45 kg	170.37 lb <sub>m</sub>
$L_d$ Overhang Distance	0.227 m	8.95 in.
$W$ Rotor Weight	1202 N	270 lbf
$U_{im}$ Initial Mech. Imbalance	0.11 kg mm	0.15 oz in.
<i>Lubricant Parameters</i>		
$P_s$ Lubricant supply pressure	0.104 MPa	1.5 psi
$T_b$ Lubricant supply temp.	50 °C	122 °F
$\beta$ Thermoviscosity index	0.031 /°C	0.017 /°F
$\mu_s$ Lubricant supply viscosity	20.3 cP	2.94 $\mu$ reyn
$\rho_s$ Lubricant density	888 kg/m <sup>3</sup>	0.031 lb <sub>m</sub> /in <sup>3</sup>
$c_p$ Lubricant sp. heat capacity	1992 J/kg/K	0.478 Btu/lb <sub>m</sub> /°F

## CONCLUSION

• A theoretical model is presented for a synchronous thermal instability prediction of overhung rotors. This model utilizes a threshold imbalance criterion for prediction of stability instead of employing the traditional frequency-domain feedback analysis. A front-end computer program, which is based on this model, was developed to calculate and analyze the thermal instability in overhung rotor systems.

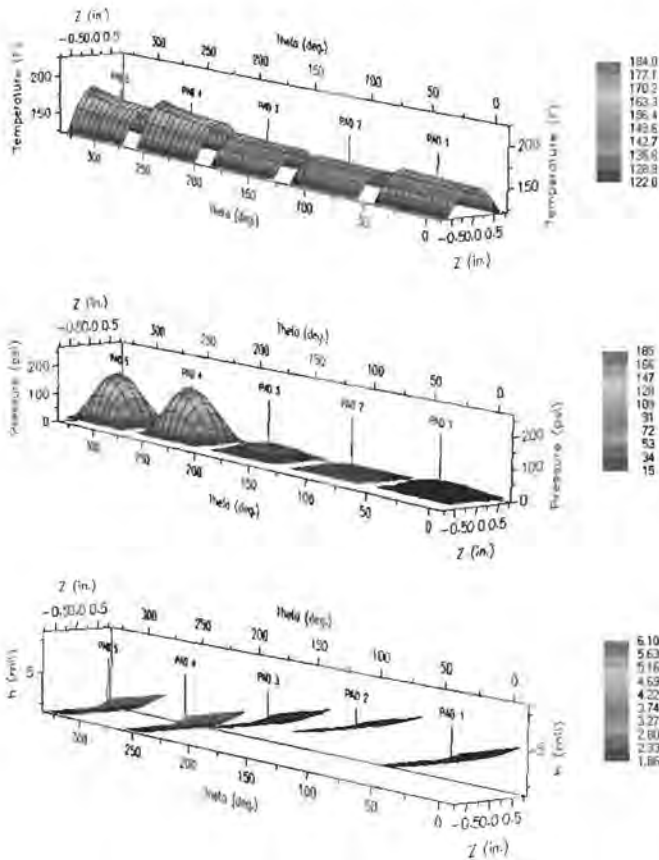


Figure 32. Temperature, Pressure, and Film Thickness at 8000 RPM,  $L/D = 0.25$ .

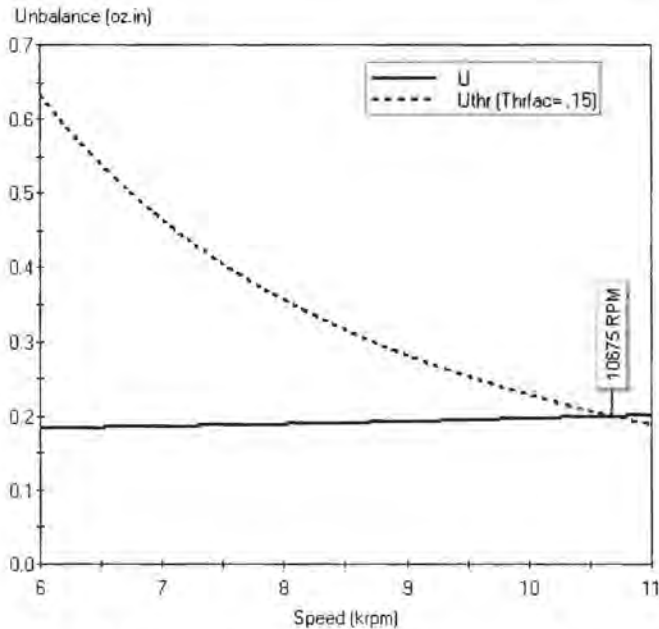


Figure 33. Stability Plot for Pipeline Compressor Rotor,  $L/D = 0.25$ .

• Two plain journal bearing rotor cases (Keogh and Morton rotor, Faulkner, Strong, and Kirk rotor) and one tilting pad journal bearing rotor case (pipeline compressor) were calculated and discussed. In general, the calculation results agree well with the practical observations.

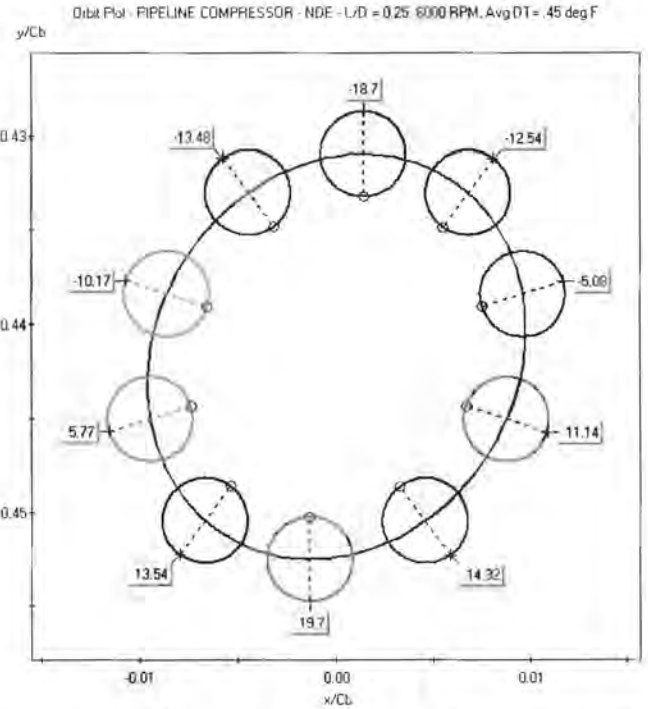


Figure 34. Orbit Plot of Pipeline Compressor Rotor at 6000 RPM,  $L/D = 0.25$ .

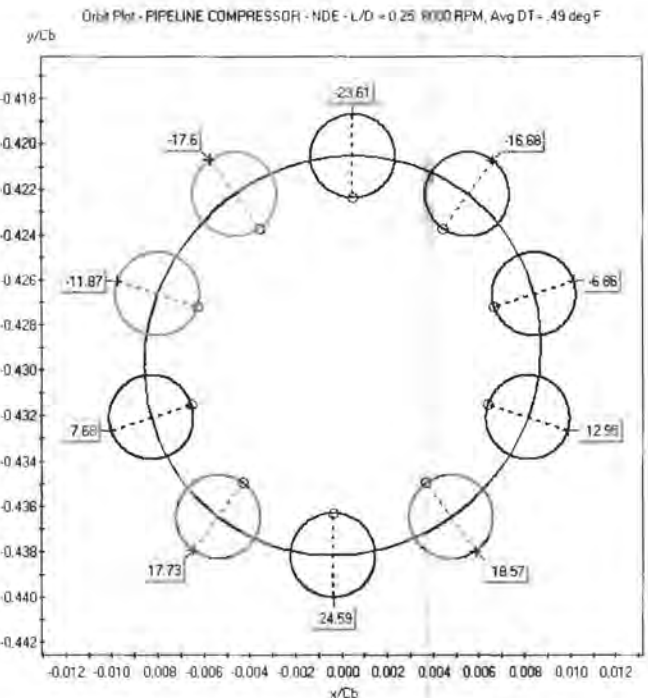


Figure 35. Orbit Plot of Pipeline Compressor Rotor at 8000 RPM,  $L/D = 0.25$ .

- Two methods to locate the hot/cold spot are discussed. The improved method is preferred in plain journal bearing calculations and is still being evaluated for tilting pad bearing analysis.
- The number of dynamic orbit points for calculating average temperature difference may influence the accuracy of the instability prediction. Based on the discussion in the Keogh and Morton case, 10 orbit points were finally considered to provide the prediction with acceptable accuracy.

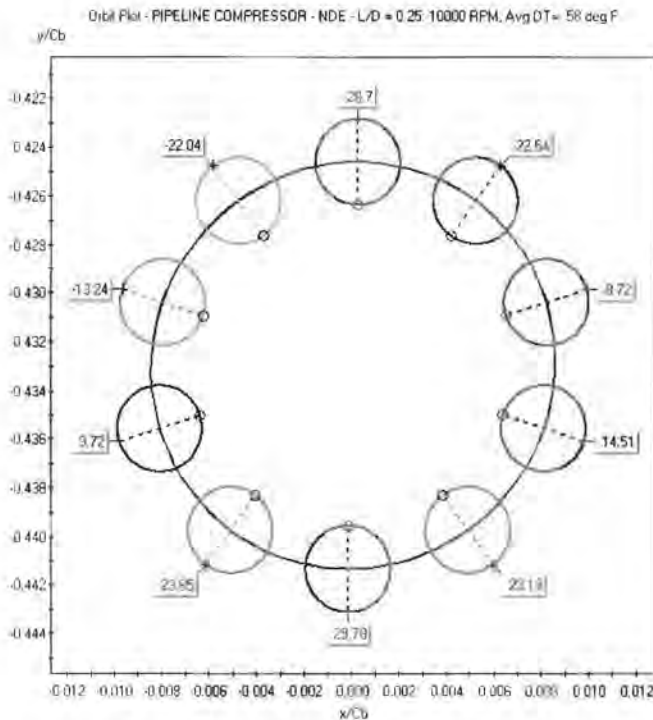


Figure 36. Orbit Plot of Pipeline Compressor Rotor at 10,000 RPM,  $L/D = 0.25$ .

• The value of the predicted thermal imbalance and the phase angle between the thermal and mechanical imbalances will influence the resultant total imbalance and, hence, the possibility of thermal instability. The worst scenario for Morton effect is achieved with a centered, circular, large amplitude orbit at high speed and having a small phase angle between the resulting thermal imbalance and the original mechanical imbalance.

## NOMENCLATURE

Dimensions: M = Mass, L = length, t = time, T = temperature

$A_x, A_y$	= Amplitude parameters for elliptic orbit (L)
$c_j$	= Lubricant specific heat capacity ( $L^2 t^{-2} T^{-1}$ )
$C_b$	= Radial bearing clearance (L)
$C_p$	= Radial pad clearance (L)
$e$	= Eccentricity (L)
$E$	= Young's modulus ( $M L^{-1} t^{-2}$ )
$\dot{E}_b$	= Rate of energy transfer to bearing ( $M L^{-2} t^{-3}$ )
$\dot{E}_j$	= Rate of energy transfer to journal ( $M L^{-2} t^{-3}$ )
$\dot{E}_{j, \text{sub}}$	= Rate of energy storage in lubricant ( $M L^{-2} t^{-3}$ )
$\dot{E}_{\text{visc}}$	= Rate of viscous energy dissipation ( $M L^{-2} t^{-3}$ )
$f_p$	= Fractional angular position of pad pivot
$h$	= Film thickness (L)
$H$	= Heat transfer coefficient ( $M t^{-3} T^{-1}$ )
$I$	= Area moment of inertia ( $L^4$ )
$L$	= Bearing length (L)
$L_d$	= Disk overhang length (L)
$m$	= Preload factor
$m_d$	= Mass of overhung disk (M)
$O_b$	= Bearing center
$O_j$	= Journal center
$O_p$	= Pad center of curvature
$P_0$	= Lubricant supply pressure ( $M L^{-1} t^{-2}$ )
$R_b$	= Bearing radius (L)
$R_j$	= Journal radius (L)
$R_p$	= Inner radius of curvature of pad (L)
$T_0$	= Lubricant supply temperature (T)
$t_p$	= Pad thickness

$T$	= Journal circumferential temperature (T)
$T_{\text{amb}}$	= Ambient temperature (T)
$U$	= Resultant imbalance (M L)
$U_m$	= Mechanical imbalance (M L)
$U_t$	= Thermal imbalance (M L)
$U_{\text{thr}}$	= Threshold imbalance (M L)
$W$	= Rotor weight ( $M L t^{-2}$ )
$W_b$	= Bearing load ( $M L t^{-2}$ )
$y_d$	= Thermal deflection of disk (L)
$z$	= Axial dimension (L)
$\alpha$	= Journal coefficient of thermal expansion ( $T^{-1}$ )
$\beta$	= Thermoviscosity coefficient ( $T^{-1}$ )
$\delta$	= Pad tilt angle
$\epsilon$	= Eccentricity ratio
$\theta$	= Circumferential angle
$\theta_c$	= Angle for line-of-centers
$\theta_j$	= Angle to journal center
$\theta_p$	= Pivot angle for pad
$\mu$	= Lubricant viscosity ( $M L^{-1} t^{-1}$ )
$\mu_0$	= Lubricant supply viscosity ( $M L^{-1} t^{-1}$ )
$\xi$	= Angle used in PJB film thickness expression
$\rho_l$	= Lubricant density ( $M L^{-3}$ )
$\tau$	= Lubricant shear stress ( $M L^{-1} t^{-2}$ )
$\phi$	= Angle between thermal and mechanical unbalances
$\phi_x, \phi_y$	= Phase parameters for elliptical orbit
$\Psi$	= Thermal bend angle
$\omega$	= Angular journal speed ( $t^{-1}$ )

## REFERENCES

- Balbahadur, A. C. and Kirk, R. G., 2002a, "Part I—Theoretical Model for a Synchronous Thermal Instability Operating in Overhung Rotors," *Proceedings of 2002 IFTOMM*, Sixth International Conference on Rotor Dynamics, September 30 to October 4, Sydney, Australia.
- Balbahadur, A. C. and Kirk, R. G., 2002b, "Part II—Case Studies for a Synchronous Thermal Instability Operating in Overhung Rotors," *Proceedings of 2002 IFTOMM*, Sixth International Conference on Rotor Dynamics, September 30-October 4, Sydney, Australia.
- Cameron, A., 1966, *The Principles of Lubrication*, London, England: Longmans Green & Co. Ltd.
- de Jongh, F. M. and Morton, P. G., 1994, "The Synchronous Instability of a Compressor Rotor Due to Bearing Journal Differential Heating," ASME Paper 94-GT-35, pp. 1-13.
- Dimarogonas, A. D., 1973, "Newkirk Effect: Thermally Induced Dynamic Instability of High-Speed Rotors," ASME Paper 73-GT-26, pp. 2-11.
- Ettles, C. M., 1992, "The Analysis of Pivoted Pad Journal Bearing Assemblies Considering Thermoelastic Deformation and Heat Transfer Effects," *Tribology Transactions*, 35, (1), pp. 156-162.
- Faulkner, H. B., Strong, W. F., and Kirk, R. G., 1997a, "Thermally Induced Synchronous Instability of a Radial Inflow Overhung Turbine, Part I," DETC97/VIB-4063, *Proceedings of 1997 ASME Design Engineering Technical Conferences*, September 14-17, Sacramento, California.
- Faulkner, H. B., Strong, W. F., and Kirk, R. G., 1997b, "Thermally Induced Synchronous Instability of a Radial Inflow Overhung Turbine, Part II," DETC97/VIB-4174, *Proceedings of 1997 ASME Design Engineering Technical Conferences*, September 14-17, Sacramento, California.
- Keogh, P. S. and Morton, P. G., 1994, "The Dynamic Nature of Rotor Thermal Bending Due to Unsteady Lubricant Shearing Within Bearing," *Proceedings of Royal Society of London, Series A*, 445, pp. 273-290.

- Kirk, R. G., Raju, K. V. S., and Ramesh, K., 1999, "PC-Based Analysis of Turbomachinery Vibration," *The Shock and Vibration Digest*, 31, (6), pp. 449-454.
- Larsson, B., 1999a, "Journal Asymmetric Heating—Part I: Nonstationary Bow," *Journal of Tribology*, 121, pp. 157-163.
- Larsson, B., 1999b, "Journal Asymmetric Heating—Part II: Alteration of Rotor Dynamic Properties," *Journal of Tribology*, 121, pp. 164-168.
- Monmousseau, P., Fillon, M., and Frene, J., 1997, "Transient Thermoelastohydrodynamic Study of Tilting-Pad Journal Bearings—Comparison Between Experimental Data and Theoretical Results," *Journal of Tribology*, 119, pp. 401-407.
- Newkirk, B. L., 1926, "Shaft Rubbing," *Mechanical Engineering*, 48, (8), pp. 830-832.
- Schmied, J., September 1987, "Spiral Vibrations of Rotors," Rotating Machinery Dynamics, 2, *ASME Design Technology Conference*, Boston, Massachusetts.

#### ACKNOWLEDGEMENT

The authors express their gratitude to Virginia Tech Rotor Dynamics Lab Industrial Affiliates Group for their interest and support of this project.